PAPER G

CALCULATION OF DIRECT ARRIVAL TRAVELTIMES: BY THE EIKONAL EQUATION

Le-Wei Mo

ABSTRACT

We present a traveltime calculation scheme based on the eikonal equation that calculates the traveltimes of direct arrivals from a point source. In typical earth models, critical refractions, diffractions and reflections are weak. Most of the energy radiated by the source is contained in the direct arrivals. Direct arrivals are thus generally the most energetic events in a time evolving wavefield. Our scheme successfully computes the travel times of direct arrivals and is computationally efficient. The travel time maps are then used to find ray paths from the receivers back to the source. The method is presented in two dimensions.

INTRODUCTION

Wave propagation in medium, in high frequency asymptotics, can be described by the WKBJ Green's function, which consists of traveltimes and amplitudes. The traveltimes satisfy the eikonal equation that relates the gradient of the traveltimes to slowness of the model. The amplitudes satisfy the transport equations. In this paper, we will address the problem of solving the eikonal equation for direct arrival traveltimes. One method of solving the eikonal equation is the method of characteristics (Cerveny et al., 1977; Zauderer, 1989). The ray equations are derived from the eikonal equation, whose solutions are raypaths or the characteristic curves of the eikonal equation. Because the raypaths are local, wave propagation along rays is thus intuitive and easy to understand. This explains why the application of ray tracing is so popular and there has been a wealth

of published information about it. However, ray tracing has its limitations and disadvantages as pointed out by some authors (Vidale, 1988). Seismic depth migration, and many other applications require traveltimes on a uniform grid. If these traveltimes are computed by ray tracing, computation cost is immense. We would rather solve the eikonal equation directly for traveltimes on a uniform grid.

Reshef and Kosloff (1986) formulated finite-difference scheme to solve the eikonal equation for traveltimes on a uniform grid by extrapolating the depth gradient of traveltimes. Vidale (1988, 1990) formulated a finite-difference scheme in Cartesian coordinates that solves the eikonal equation progressing outward from an ``expanding square'' for traveltimes of first arriving waves from a point source. His scheme can quickly fills in traveltimes in a uniform grid, and is by far the fastest method of computing traveltime. However, Vidale's scheme encounters stability problems, e.g., calculating the square root of a negative number. Qin et al. (1992) proposed an alternate of Vidale's scheme, i.e., progressing outward from an ``expanding wavefront.'' Qin et al.'s scheme solves some of the stability problems of Vidale's algorithm. But searching for the global minimum to start computation at each step makes their scheme computation costly. Podvin and Lecomte (1991) dissected wave propagation in a cell into all possible modes of transmission, diffraction and head waves, resulting in a stable scheme of traveltime calculation. Van Trier and Symes (1991) formulated traveltime calculation in polar coordinates by extrapolating the gradients of traveltimes. In their schemes, traveltime computation has the contradiction of dense sampling near the source and coarse sampling far away from the source. And mapping the slowness and traveltime fields to and from polar coordinates requires additional computation cost. As a matter of fact, efficiency of a traveltime computation scheme also depends on the computer architecture. But Vidale's scheme requires the least number of algebraic operations.

The common shortcoming of the above finite-difference traveltime calculation schemes is that they all explicitly or implicitly calculate traveltime of first arriving waves, which may carry very little energy and are very weak, e.g., head waves and diffractions. In this paper, we propose a traveltime calculation scheme that aims at calculating the traveltimes of direct arrivals from a point source. In typical earth models, diffraction and reflection effects are weak. Most of the energy radiated by the source is contained in the direct arrivals. Direct arrivals are thus generally the most energetic events in a time evolving wavefield. First, we analyze why we prefer direct arrival traveltimes to first arrival traveltimes in tomography and migration imaging. Then we present our scheme of

calculating direct arrival traveltimes. Finally, we show several numerical examples of calculating direct arrival traveltimes. Our scheme successfully computes the traveltimes of direct arrivals and is computationally efficient. The method is presented in two dimensions.

WHY DIRECT ARRIVAL TRAVELTIMES

Figure 1(b) shows the snapshot wavefield at 0.16 seconds of a two layer velocity model of Figure 1(a). The wavefield is simulated by the finite-difference solution to the scalar wave equation. The source is at the upper left corner. The source wavelet is the first derivative of the Gaussian function. For this model, head wave is generated and part of its travel path is the boundary separating the slow and the fast medium. The head wave is a boundary wave, and carries very little energy. Figure 1(c) is the common shot gather or history wavefield of receivers at the right edge of Figure 1(b). From Figure 1(b) and (c), we see that the first arrival - head wave, travels ahead of the direct arrival and is much weaker than the direct arrival. If the traveltimes of the head wave in the slow medium were used for transmission traveltime tomography, the slow velocity medium would be inverted as an erroneous high velocity medium. And reflections that are used by migration to image velocity discontinuities are not generated by the first arrival head wave. Thus traveltimes of the first arrival - head wave, are not suitable as inputs for transmission traveltime tomography and migration imaging. In stead, traveltimes of direct arrivals should be used. Overlay on Figure 1(b) and (c) are the direct arrival traveltimes computed by our finite-difference scheme of solving the eikonal equation. The direct arrival traveltimes closely match the first breaks of the direct arrivals computed by finite-difference wave equation modeling.

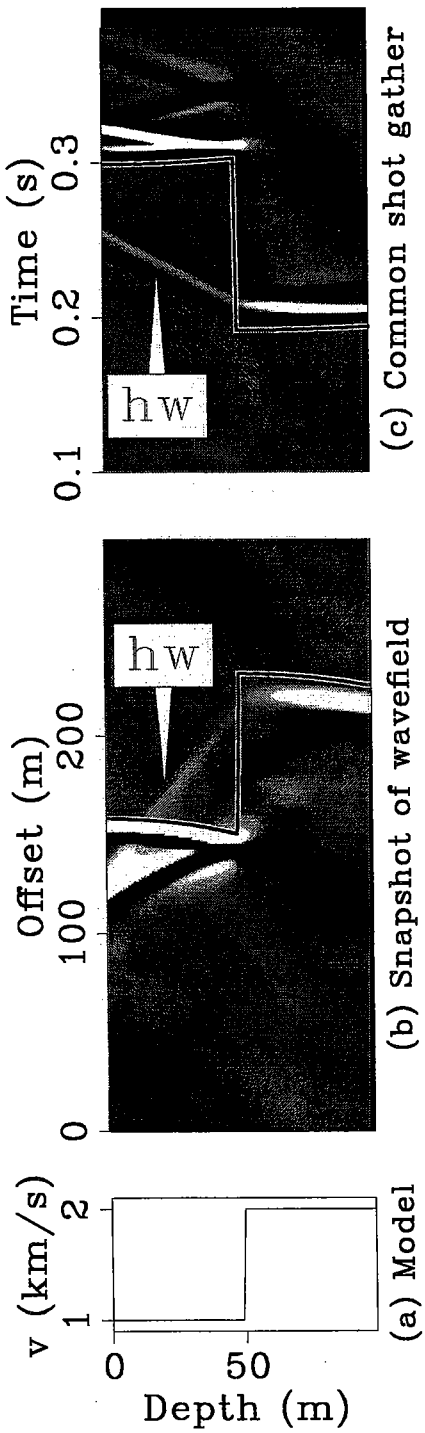

Figure 1. (a) is the 1-D velocity model. In (b), source is at the upper left corner.(c) is the common shot gather with receivers at the right edge of (b). The label "hw" point to the head wave event, which is much weaker than the primary reflection.

RAY TRACING

Figure 2 is a two layer velocity model. The lower medium has higher velocity. By ray tracing, the incidence ray at point C is in critical incidence and generates a creeping ray along the boundary. The incidence rays to the left of point C, e.g., at point A, are in pre-critical incidence and generate refracted waves in the lower medium. The incidence rays to the right of point C, e.g., at point B, are in post-critical incidence, and total reflection occurs. For post-critical incidence rays, the symptoms are the sine of the refraction angle is greater than 1 and the incidence wavefront in the slow medium and the creeping wavefront in the fast medium are discontinuous across the interface. Transmission ray tracing can be performed for pre-critical incidence rays to the left of point C. However, transmission ray tracing can not be performed for post-critical incidence rays to the right of point C. That is, transmission ray tracing is performed only until total reflection occurs, or until the sine of the refraction angle is greater than 1.

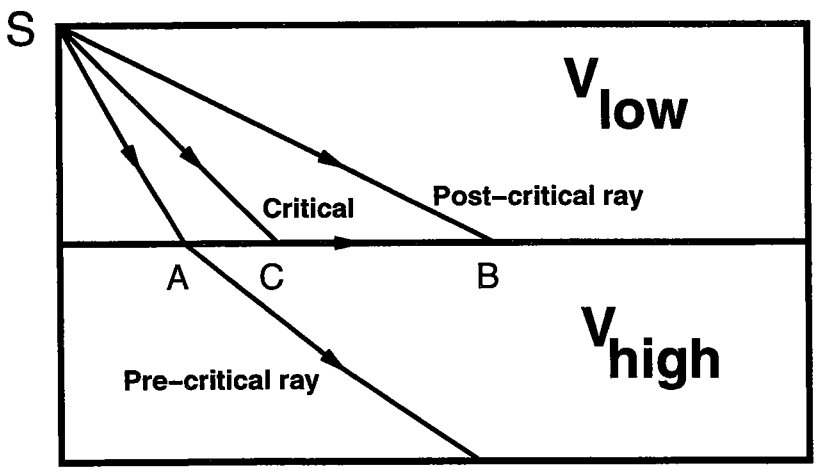

Figure 2. Incidence ray at point C is in critical incidence. Incidence ray at A (B) is in pre-critical (post-critical) incidence.

SOLVING THE EIKONAL EQUATION

In a two dimensional medium, the traveltime of wave propagation is governed by the eikonal equation, which relates the gradient of traveltimes to the slowness of the medium,

$$(\frac{\partial t}{\partial x})^2 + (\frac{\partial t}{\partial z})^2 = s^2(x,z) \tag{1}$$

where *(x,z)* is spatial coordinate, *t* is traveltime, *s(x,z)* is slowness. We parameterize the medium by square cells, with mesh spacing *h*, Figure 3. In a localized cell of Figure 3, when traveltimes at three corners *a, b* and *c* are known, the traveltime at the fourth corner -- *d* can be found by finite-difference method based on the assumption of local plane wave. We use the centered finite-difference (Vidale, 1988) to approximate the two differential terms in equation (1)

$$\frac{\partial t}{\partial x} = \frac{1}{2h}(t_b + t_d - t_a - t_c) \tag{2}$$

and

$$\frac{\partial t}{\partial z} = \frac{1}{2h}(t_c + t_d - t_a - t_b) \tag{3}$$

Substituting equations (2) and (3) into equation (1) gives

$$t_d = t_a + \sqrt{2(hs)^2 - (t_b - t_c)^2} \tag{4}$$

where h is mesh spacing, s is the slowness inside the cell with the grid indexes of corner d, t_a, t_b, t_c and t_d are the traveltimes at the corners a, b, c and d. Finite-differences in equations (2) and (3) have second order of numerical accuracy.

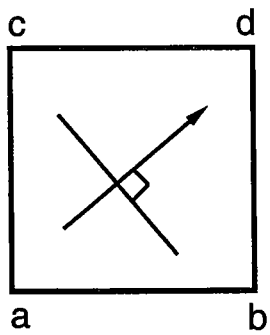

Figure 3. In a square cell with constant slowness *s*, wave propagates from corner *a* to corner *d* through corners *b* and *c*. Traveltime is larger at corner *b* than at corner *a*.

Equation (4) can only be used for traveltime calculation at pre-critical incidence. At post-critical incidence, the problem is to compute the square root of a negative number. But setting the negative number inside the square root to zero (Vidale, 1988, 1990) does not conform to physics. When geometrical ray theory is valid and the wavefronts are continuous across an interface, the time difference between diagonal nodes of a square cell is at most $\sqrt{2}hs$, where h is the mesh spacing of the cell and s is the slowness inside the cell. Thus there are three equivalent symptoms of post-critical incidence, the sine of the refraction angle being greater than 1, wavefronts being discontinuous across an interface and the time difference between diagonal nodes of a square cell being greater than $\sqrt{2}hs$ Thus in solving the eikonal equation, the term inside the square root of equation (4) is negative at post-critical incidence. The method to handle post-critical incidence traveltime computation is depicted in Figure 4. If corners a and b lie in a horizontal direction and wave travels from a to b, then corners a and b are in the slow velocity medium, and corners c and d are in the high velocity medium. In geometric ray theory, the direct arrival to corner d is a creeping ray from corner c to corner d. The traveltime at corner d is then computed as

$$t_d = t_c + hs \tag{5}$$

If corners a and b lie in a vertical direction and wave travels from a to b, the direct arrival to corner d is a creeping ray from corner b to corner d. The traveltime at corner d is then computed as

$$t_d = t_b + hs \tag{6}$$

We have described the traveltime computation at a localized cell. Next, we describe the arrangement of computation patterns.

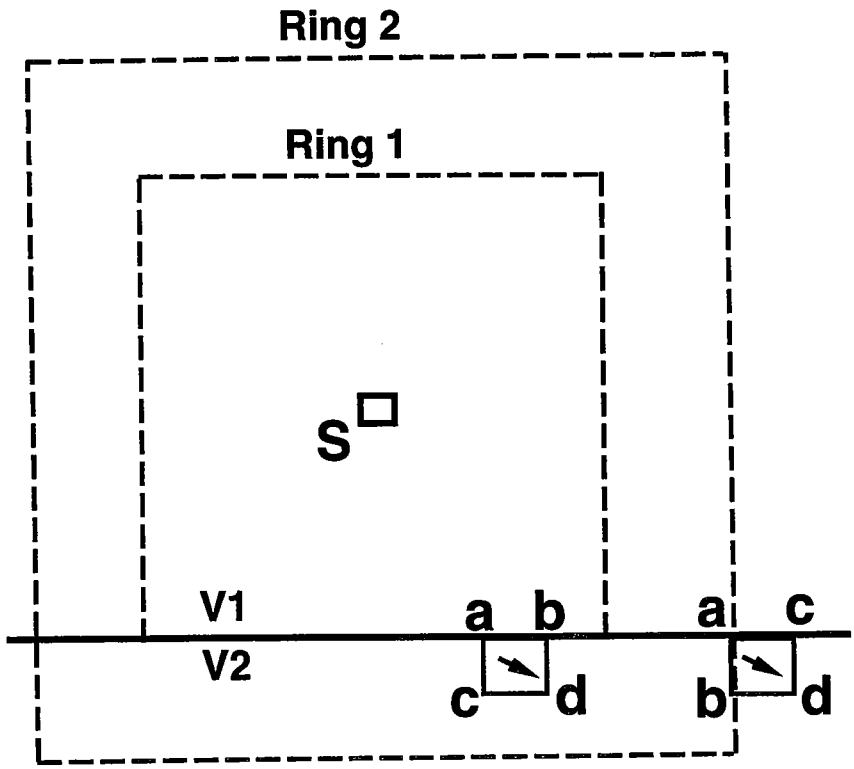

Figure 4: Depending on the horizontal and vertical orientations of the inner edge of a square cell, the way to compute boundary creeping wave travel time is different.

COMPUTATION PATTERN

Traveltime computation is initialized by assuming straight ray paths in a constant velocity square surrounding the source point. We found the radius of $5h$ to be a generally good choice for the initialization square. Traveltime computations are then carried out by expanding squares around the source point, as the computation layout in Figure 6. The filled circles indicate grid points that have had their traveltimes calculated. We are to use the traveltimes at the boundary ring of grid points, large filled circles, to compute traveltimes of grid points at an outer ring, the hollow circles. The inductive scheme for calculating a new ring of traveltimes is now described. Computations proceed sequentially on the four sides, as shown in Figure 6 (Podvin and Lecomte, 1991). To initialize computation at a side, the points in the inner side are examined in a loop from one end to the other to locate the point with local minimum traveltime. Using one-sided finite-difference stencil, the traveltime of the point outside the point with local minimum traveltimeis computed as

$$t_c = t_a + \sqrt{(hs)^2 - (t_b - t_a)^2} \tag{7}$$

where t_c is the time to be found, t_a is the local minimum traveltime in the inside row, t_b is the traveltime of the neighboring grid point at the source side, s is the slowness at point c. However, if the term inside the square root of equation (7) is negative, the traveltime at point c is computed as

$$t_c = t_a + hs \tag{8}$$

At the next stage, equation (4) is applied to compute traveltimes.

In application of equation (4), the propagation direction of local plane wave does not come in play. The traveltimes at the three corners a, b and d can also be used to compute the traveltime at corner c because of the assumption of local plane wave. Equations (5) and (6) are then changed by computing the right hand side unknown traveltime from the left hand side known traveltime. However, it is easy to program calculation from small traveltimes to large traveltimes, i.e., in a upwind format.

Consider calculating traveltimes at side 1 (top) of Figure 6. Application of equation (4) is carried out in three loops, as shown in Figure 5. The first loop progresses from the left end to the lateral location of the source. Then the second loop progresses from the right end to the left end. Finally the third loop progresses from the lateral location of the source to the right end. During each loop, calculation starts at each local minimum traveltime point and progresses until a local maximum traveltime point is reached. Similar traveltime calculations are carried out sequentially for the other three sides.

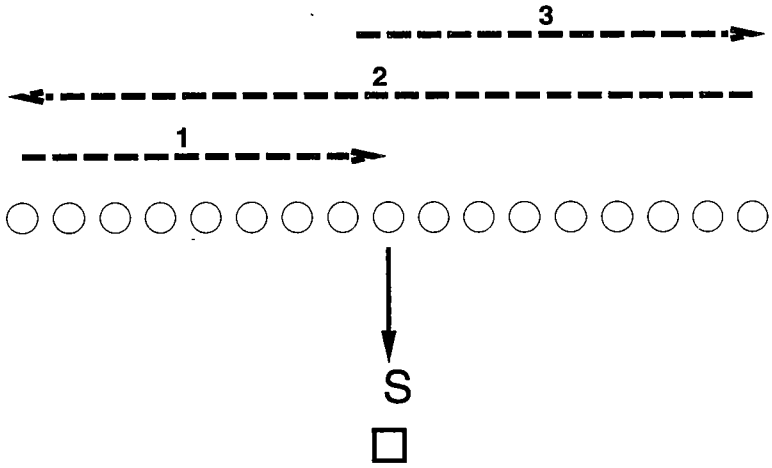

Figure 5: Travel time compuation at an edge is carried out in three separate loops, as shown, loop 1, 2 and 3.

As shown in Figure 6, the start and end point indices of the computation layouts are not the same for the fours edge. Thus, the computed travel times show artificial anisotropy even for isotropic velocity models. To solve this problem, we need to rotate the first of the four edges to start computation. For example, in Figure 6 we perform computation sequentially at the top, right, bottom and left edges, then at the next ring we perform computation sequentially at the right, bottom, left and top edges.

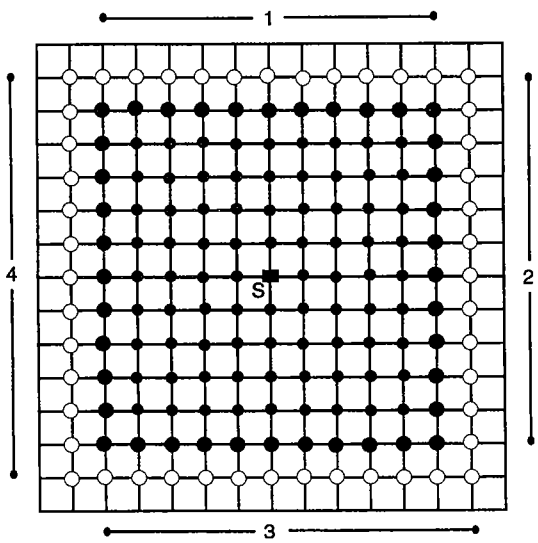

Figure 6. *S* is the source grid point. Traveltime computations proceed sequentially on the four sides.

EXAMPLE

Figure 7 shows in the grey-scale background a complicated 1-D velocity model, it also shows the traveltime contours of direct arrivals with the source at the upper left corner. All the possible direct arrivals in 1-D medium are correctly modeled. It has transmission from high velocity medium to low velocity medium, transmission and creeping boundary wave from low velocity medium to high velocity medium, and overturning waves in medium with linear increasing velocities. Figure 8 overlies a snap-shot wavefield computed by finite-difference wave equation modeling with the corresponding direct arrival traveltimes computed by our eikonal equation solver. There is a close match between the traveltimes and the waveforms.

Figure 9 shows a 2-D velocity model and the traveltime contours of direct arrivals. Figure 10 shows a wave equation modeling snap-shot wavefield and the corresponding direct arrival traveltime contour. The transmissions from high velocity medium to low velocity medium, and from low velocity medium to high velocity medium are correctly described. However, there are some jitters on the traveltime contours along the 45-degree direction from the source, which is owing to shifting computation from one square-ring to another, but the wavefront expands circularly from the source.

A POSTERIORI RAY TRACING

After travel times have been computed for all the grid nodes, ray path from any receiver grid point back to the source can be traced by following the steepest descent direction through the travel time field. The ray paths are guaranteed to end at the source point as the source point has the smallest travel time, zero. The gradient direction in a cell are computed by using the following finite-difference equations and using the labels in Figure 3:

$$\frac{\partial t}{\partial x} = -\frac{1}{2h}(t_b + t_d - t_a - t_c) \tag{9}$$

and

$$\frac{\partial t}{\partial z} = \sqrt{s^2 - \left(\frac{\partial t}{\partial x}\right)^2}\, signum(t_c + t_d - t_a - t_b) \tag{10}$$

Equation (9) is different from equation (2), because in ray tracing we are following the backward direction of the ray path. The z derivative computed in the above equation (10) guarantees that pre-critical, critical, and post-critical ray paths are correctly handled.

Figure 11 shows the ray paths calculated on the McElroy near offset travel time tomogram. In this case, thousands of ray paths can be computed in two or three minutes. I just display 10 of them to reduce the size of the figure.

DISCUSSIONS

In this traveltime calculation scheme, the velocity model is parameterized as constant velocity cells. For one-dimensional velocity medium, it is perfect. For two-dimensional velocity medium, dipping interfaces are represented by stairways. The other source of inaccuracy is the computation square front differing from the actual circular expanding wavefront.

As seen in Figures 1, 8 and 10, the calculated direct arrival traveltimes closely match the waveforms of wave equation modeling. We are confident that the direct arrival traveltimes calculated by our scheme are accurate up to the spatial and temporal sampling requirements in traveltime tomography and seismic migration.

The computational cost of this scheme at each grid point is to evaluate equation (4). For a model of realistic size, say 250,000 grid points, computational time is just a few seconds at a present workstation with computation speed of Mflops/s. Also traveltime computations are carried out in a few well defined loops as explained in the section of computation pattern, this traveltime computation scheme can easily put into a vector computer.

CONCLUSIONS

Direct arrivals are usually the most energetic events in a time evolving wavefield. Traveltimes of direct arrivals are what are used in transmission traveltime tomography and migration imaging. Our new scheme of finite-difference solving the eikonal equation successfully computes the traveltimes of direct arriving waves. And the computed traveltimes closely match the waveforms from finite-difference wave equation modeling.

By incorporating the wave propagation phenomena in the process of travel time computation, we are guaranteed that the method is stable. And by circulating the order of travel time computations at the four edges of the computation expanding ring, we are guaranteed that there is no artificial anisotropy in the computed travel time maps. The aposteriori ray tracing methods can compute pre-critcal, critical, and post-critical incidence ray paths. The methods presented can efficiently compute travel time maps and direct arrival ray paths, they can be applied in Kirchhoff depth migration, travel time tomography, and interactive seismic data processing.

REFERENCES

Cerveny, V., Molotkov, I. A., and Psencik, I., 1977, Ray method in seismology: Karlova Univerzita, Prague.

Podvin, P., and Lecomte, I., 1991, Finite difference computation of traveltimes in very contrasted velocity models: a massively parallel approach and its associated tools: Geophys. J. Int., **105** 271-284.

Qin, F., Luo, Y., Oslen, K. B., Cai, W., and Schuster, G. T., 1992, Finite-difference solution of the eikonal equation along expanding wavefronts: Geophysics, **57,** 478-487.

Reshef, M., and Kosloff, D., 1986, Migration of common-shot gathers: Geophysics, **51** 324-331.

Van Trier, J., and Symes, W. W., 1991, Upwind finite-difference calculation of traveltimes: Geophysics, **56**, 812-821.

Vidale, J., 1988, Finite-difference calculation of travel times: Bull. Seism. Soc. Am., **78,** no. **6**, 2062-2076.

Vidale, J., 1990, Finite-difference calculation of travel times in 3-D: Geophysics, **55,** 521-526.

Zauderer, R., 1989, Partial Differential Equations of Applied Mathematics: John Wiley and Sons.

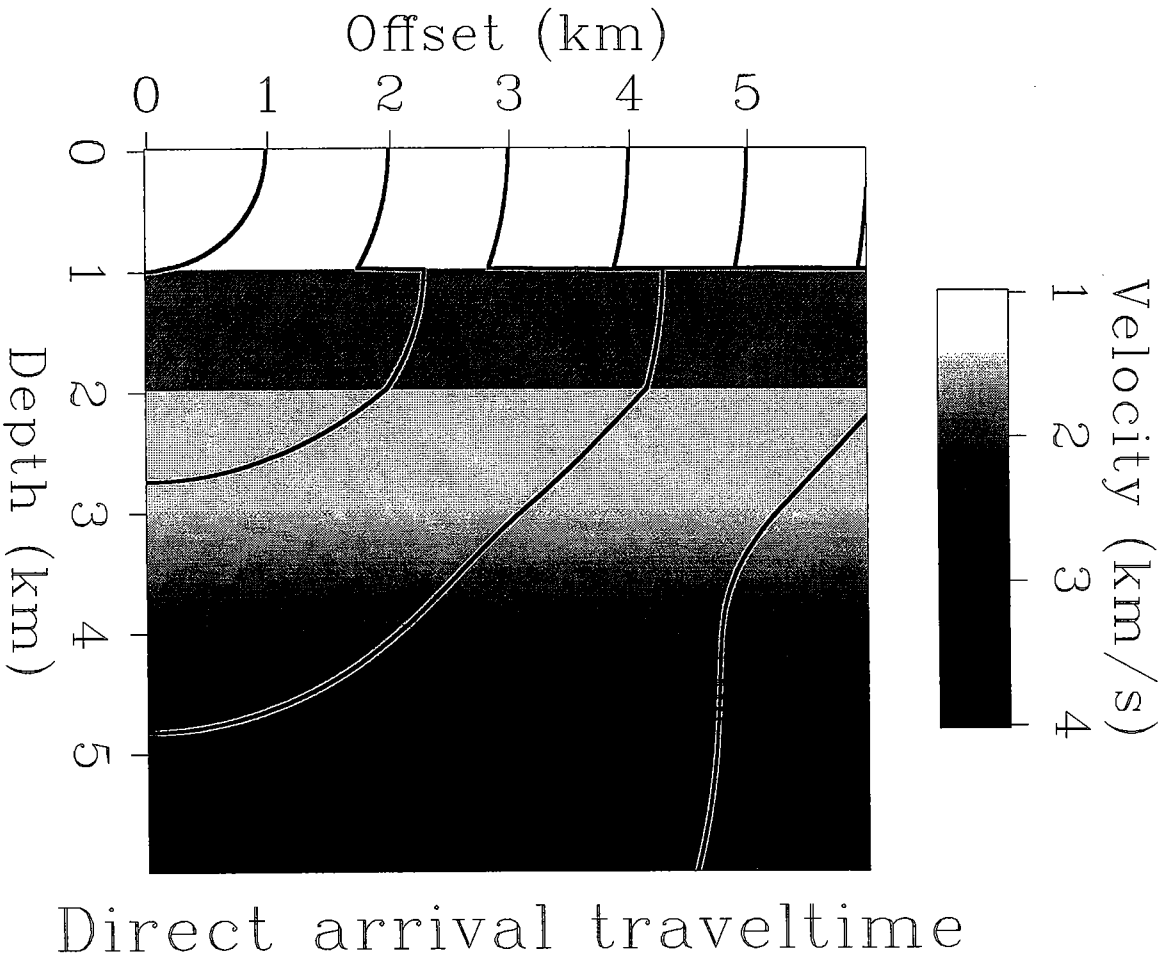

Figure 7: Shown at the grey-scale background is a 1-D velocity model. The contours are the direct arrival traveltimes from a source at the upper left corner.

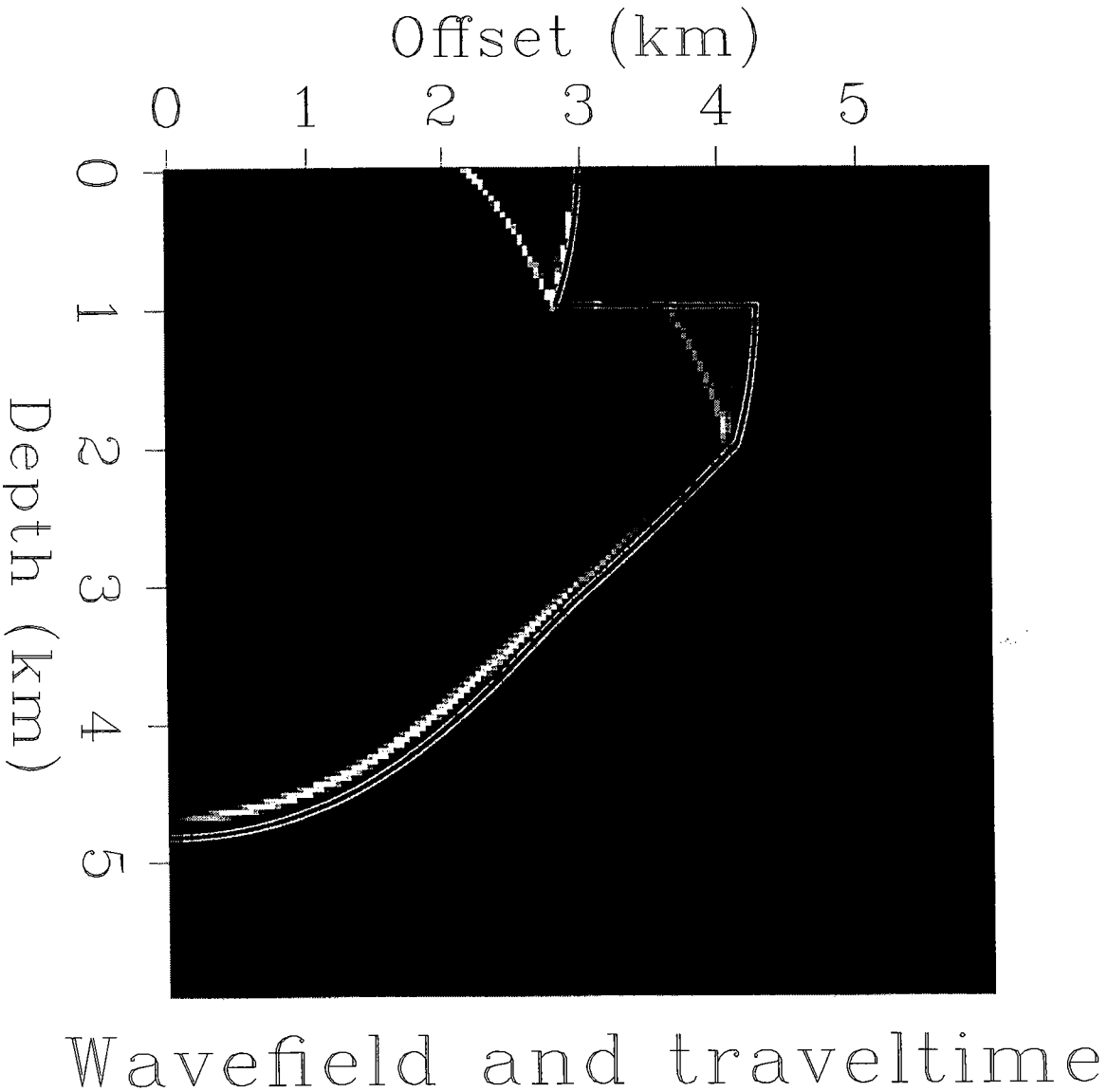

Figure 8: Comparison of the calculated direct arrival traveltimes and the snap-shot wavefields calculated by finite-difference wave equation modeling.

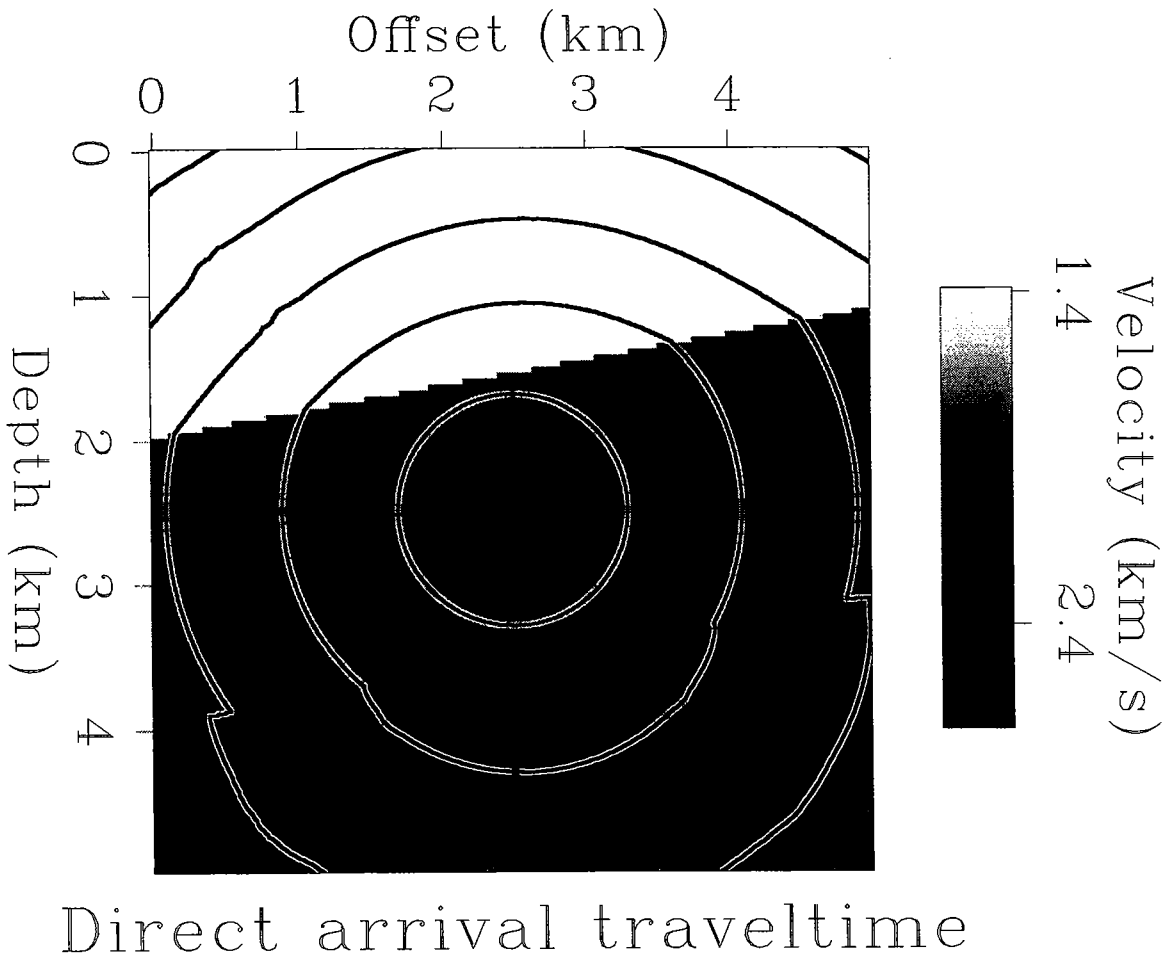

Figure 9: Shown at the grey-scale background is a 2-D velocity model. The contours are the direct arrival traveltimes from a source at the center of the model.

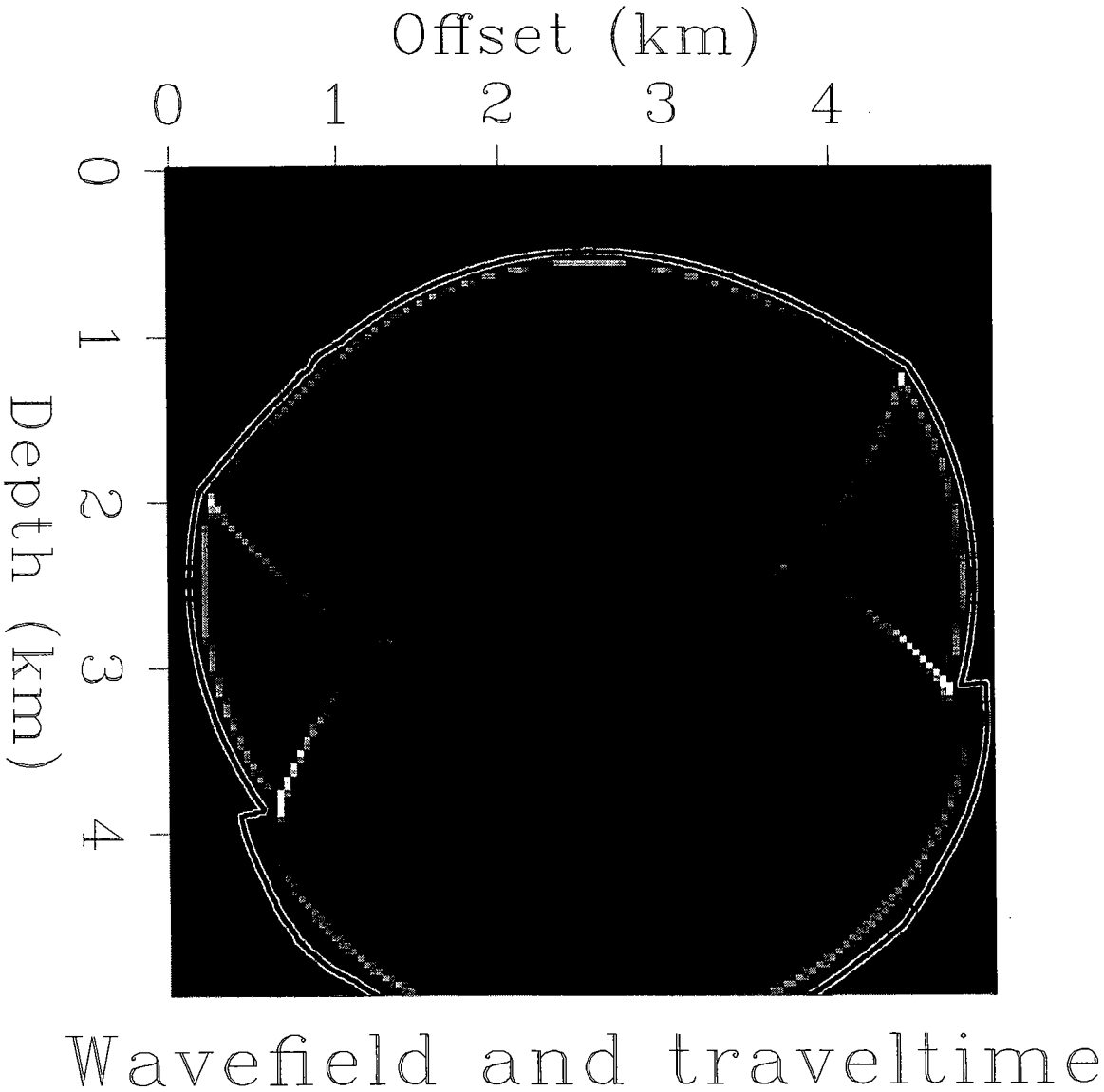

Figure 10: Comparison of the calculated direct arrival traveltimes and the snap-shot wavefields calculated by finite-difference wave equation modeling.

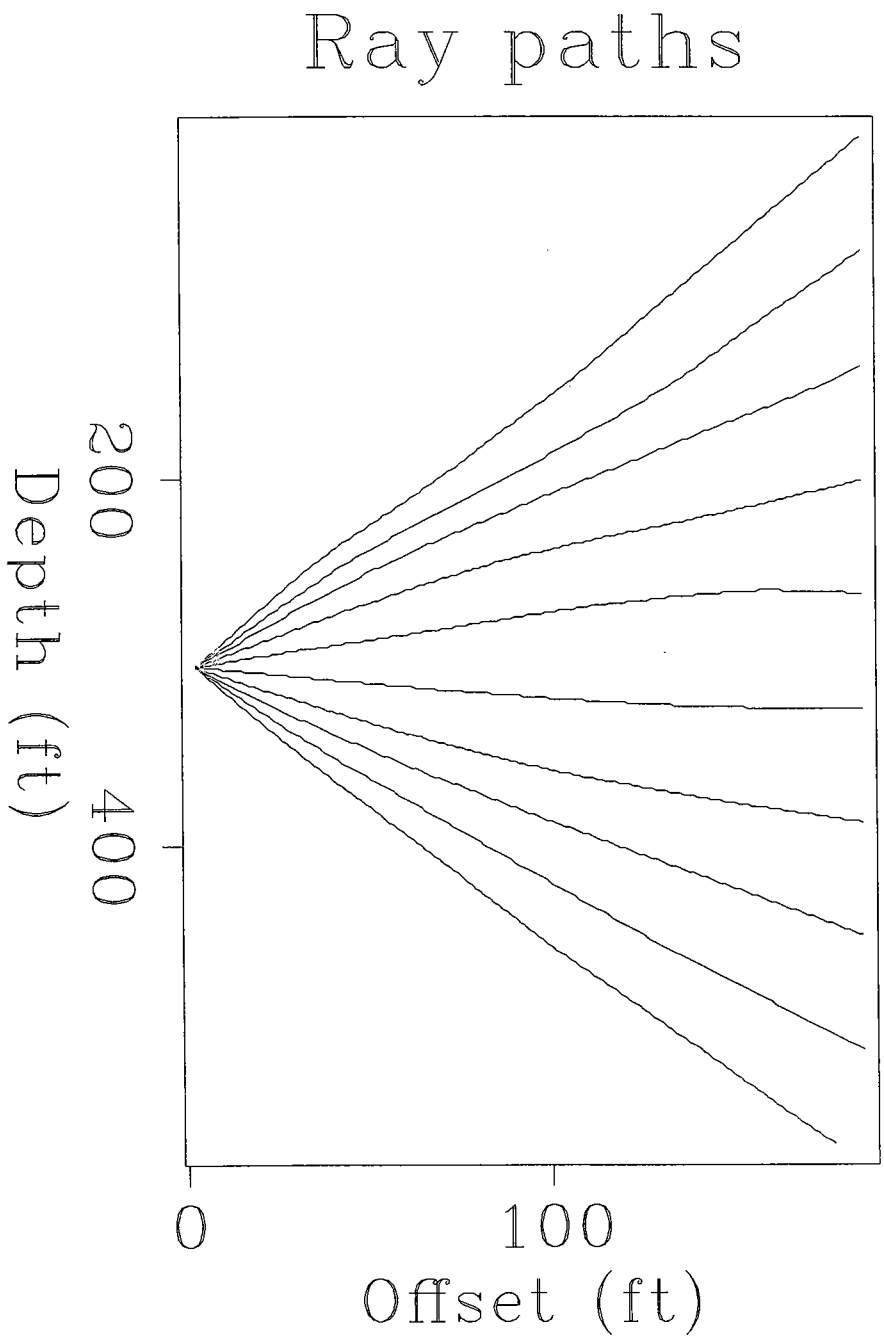

Figure 11: A fan of direct arrival ray paths calculated by aposteriori ray tracing. The model is the McElroy near offset travel time tomogram. Thousands of ray paths can be computed in a minute. I display only 10 ray paths to reduce the size of the figure.